Environmental Pollution 291 (2021) 118191

Contents lists available at ScienceDirect

Environmental Pollution

journal homepage: www.elsevier.com/locate/envpol

The effect of Covid-19 lockdown on airborne particulate matter in Rome, Italy: A magnetic point of view☆

Aldo Winkler [a,*], Antonio Amoroso [b], Alessandro Di Giosa [b], Giada Marchegiani [b]

[a] Istituto Nazionale di Geofisica e Vulcanologia, Via di Vigna Murata, 605, 00143, Rome, Italy
[b] ARPA Lazio, Regional Environmental Protection Agency, Rome, Italy

ARTICLE INFO

Keywords:
COVID-19 lockdown
Airborne particulate matter
Urban traffic
Brakes emissions
PM_{10} filters
Magnetic monitoring

ABSTRACT

Between 9 March and 18 May 2020, strict lockdown measures were adopted in Italy for containing the COVID-19 pandemic: in Rome, despite vehicular traffic on average was more than halved, it was not observed a evident decrease of the airborne particulate matter (PM) concentrations, as assessed by air quality data.

In this study, daily PM_{10} filters were collected from selected automated stations operated in Rome by the regional network of air quality monitoring: their magnetic properties – including magnetic susceptibility, hysteresis parameters and FORC (first order reversal curves) diagrams - were compared during and after the lockdown, for outlining the impact of the COVID-19 measures on airborne particulate matter.

In urban traffic sites, the PM_{10} concentrations did not significantly change after the end of the lockdown, when vehicular traffic promptly returned to its usual levels; conversely, the average volume and mass magnetic susceptibilities approximately doubled, and the linear correlation between volume magnetic susceptibility and PM_{10} concentration became significant, pointing out the link between PM_{10} concentrations and the increasing levels of traffic-related magnetic emissions.

Magnetite-like minerals, attributed to non-exhaust brakes emissions, dominated the magnetic fraction of PM_{10} near urban traffic sites, with natural magnetic components emerging in background sites and during exogenous dusts atmospheric events.

Magnetic susceptibility constituted a fast and sensitive proxy of vehicular particulate emissions: the magnetic properties can play a relevant role in the source apportionment of PM_{10}, especially when unsignificant variations in its concentration levels may mask important changes in the traffic-related magnetic fraction.

As a further hint, increasing attention should be drawn to the reduction of brake wear emissions, that are overcoming by far fuel exhausts as the main particulate pollutant in traffic contexts.

1. Introduction

On 9 March 2020, in response to the COVID-19 pandemic, in Italy it was imposed a strict national lockdown, that limited the movement of the population except for proven work needs, emergencies, or health reasons, banning non-essential travels, closing the most of commercial and retail businesses and suspending lessons at schools and Universities.

On 18 May 2020 the strictest lockdown phase ended, with the opening of all the economic activities and gradually allowing travels between regions: excluding a few days of firm measures around Christmas (24–27 December, 31 December, 1–3 and 5–6 January 2021) and Easter (3–5 April 2021, with more severe rules from 15 March), the limitations were never as rigorous as in the period 9 March 2020–18 May 2020.

The lockdown provided a unique experiment for assessing the impact of human activities on anthropic emissions, considering their unprecedent reduction from road transport, aviation, and industrial activities: the EEA Report No 9/2020 stated that NO_2 concentrations were considerably reduced across Europe in April 2020, especially where lockdown measures were more severe, including Italy.

PM_{10} concentrations were generally reduced too, although less than NO_2; the relative reduction over Italy was estimated as 35%, even if increased PM_{10} concentrations in localized areas and a general uncertain assessment of their levels suggested that other sources of natural and

☆ This paper has been recommended for acceptance by Dr. Da Chen.

* Corresponding author.
E-mail address: aldo.winkler@ingv.it (A. Winkler).

https://doi.org/10.1016/j.envpol.2021.118191
Received 9 July 2021; Received in revised form 12 September 2021; Accepted 15 September 2021
Available online 15 September 2021
0269-7491/© 2021 The Authors. Published by Elsevier Ltd. This is an open access article under the CC BY-NC-ND license (http://creativecommons.org/licenses/by-nc-nd/4.0/).

anthropic emissions, together with particulate resuspension, contributed to PM_{10}.

In Northern Italy, Putaud et al. (2021) showed that PM_{10} concentrations were not significantly affected by the lockdown measures, and that the decrease of traffic-related PM_{10} was compensated by its increase in association with wood burning for domestic heating; in Milan, PM_{10} concentrations were influenced by non-urban and non-traffic sources until May, when domestic heating was reduced and the relaxation of the containment measures led urban PM_{10} concentrations to increase.

Rovetta (2021) concluded that in Lombardy the average concentration of PM_{10} during the lockdown significantly increased compared to 2019, despite the massive blockage in the circulation of vehicles, proving that other factors heavily affected the air quality.

In Donzelli et al. (2020), there were no significant reductions in PM_{10} levels during the lockdown period in Tuscany; in Gualtieri et al. (2020), eight of the most populated cities in Italy were analyzed in the period 24 February to 30 April 2020, concluding that PM_{10} decreased up to 31.5% in Palermo and increased up to 7.3% in Naples; in Rome, PM_{10} reduced for about the 12% with respect to the same period in 2019, both at urban traffic and suburban background stations.

In this debated and controversial scenario, complementary analyses for the interpretation of PM concentration data are useful to better outline the impact of the restrictions on air quality: in this study, the magnetic properties of PM_{10} filters were investigated to compare their traffic-related metallic fractions during and after the lockdown in Rome, Italy.

In fact, PM can show remarkable magnetic properties arising from magnetite-like ferrimagnetic particles (e.g. Flanders, 1994), often associated with heavy metals (Georgeaud et al., 1997; Hunt et al., 1984); the magnetic properties of PM may arise from exhaust emissions related to industry, domestic heating, or vehicles, as well as from non-exhaust abrasion dusts from tyres and brakes (e.g., Hoffmann et al., 1999; Jordanova et al., 2004). In urban areas, motor vehicles represents the main source of magnetic PM (Szönyi et al., 2007, 2008; Sagnotti et al., 2009; Gonet and Maher, 2019), mostly emitted by the abrasion of disk brakes (Revuelta et al., 2014, Winkler et al., 2020, Chaparro et al., 2020, Gonet et al., 2021a, b).

Numerous studies were addressed to the magnetic properties of PM_{10} filters (e.g. Shu et al., 2001; Muxworthy et al., 2001, 2002; 2003; Spassov et al., 2004; Petrovský et al., 2020; Castaneda-Miranda et al., 2014; Rachwał et al., 2020; Leite et al., 2021): Sagnotti et al. (2006) made an extensive magnetic survey of the filters from air monitoring stations in Rome, aimed at the discrimination of local natural and anthropogenic sources.

Rock magnetism was extensively used also for biomonitoring airborne pollution using tree leaves, barks, mosses and lichens, being efficient PM receptors; for a review, see Hofman et al. (2017), thereinafter, Winkler et al. (2019), Marié at al. (2020): the magnetic properties of PM filters and bioaccumulators depend on the concentration and the grain-size of magnetite-like minerals accumulated on the samples, with the magnetic susceptibility being the fastest and most used parameter (Kapper et al., 2020).

This study reports a detailed rock magnetism study of the PM_{10} filters continuously collected during the lockdown and at discrete time intervals after the lockdown at three urban traffic, one suburban and one rural background monitoring stations operated in Rome by ARPA Lazio, the regional agency for environmental protection.

The testing hypothesis was that, in traffic urban stations, the magnetic properties of PM_{10} filters changed after the end of the strictest COVID-19 containment measures, when vehicular traffic promptly returned to its usual levels.

2. Methods

2.1. Location and sampling

PM_{10} filters were collected at five representative stations (Fig. 1), selected for the full availability of filters during the lockdown: Fermi (lat. = 41.863993, long. = 12.469570, height = 17 mamsl) and Magnagrecia (lat. = 41.883075, long. = 12.508950, height = 37 mamsl) are traffic stations, located in very busy roads; Cinecittà (lat. = 41.857716, long. = 12.568652, height = 48 mamsl) is a moderate traffic station located in the courtyard of a school facing a secondary road; these stations are all located in the south and southeastern sides of Rome, inside densely populated districts with tall buildings for residential and commercial land uses.

Castel di Guido (lat. = 41.889451, long. = 12.266327, height = 66 mamsl) and Sant'Agostino (lat. = 42.159983, long. = 11.742706, height = 11 mamsl) represent suburban and rural background stations, respectively: the first one is administratively in Rome, not far from the Aurelia provincial road and shortly outside the Grande Raccordo Anulare (GRA), a ring-shaped 68.2 km long motorway that encircles Rome; the second one is in a coastal locality about 60 km far from Rome, near a nature reserve.

The stations were all equipped with certified SWAM5a FAI DC dual channel Beta-attenuation PM_{10} concentration monitors: detailed equipment manuals and site descriptions are available at: https://www.arpalazio.it/web/guest/ambiente/aria/sistema-di-monitoraggio.

After collecting and measuring the magnetic properties of the lockdown filters, the sampling was extended to the following months, recovering the discrete series of filters that were still available after providing official air quality data.

In Fermi, PM_{10} filters were collected for most of the lockdown period (23 March – 18 May 2020); two more time series were analyzed afterwards, soon after the end of the measures (19 May– 14 June 2020) and nine months later (7 March −15 April 2021).

In Cinecittà, the collection of lockdown PM filters was followed by the 20 May – 14 June 2020 period.

Magnagrecia was sampled continuously from 26 March to 11 May 2020; several shorter time series were available in 2020 (9 June – 15 June, 11 October – 26 October, 15 December −29 December) and 2021 (24 January – 28 January, 18–22 February, 11–22 March).

Castel di Guido filters were continuously collected from 29 March to 14 June 2020, similarly to Sant'Agostino, sampled from 20 March to 14 June 2020.

2.2. Magnetic measurements

The low-field magnetic susceptibility of PM_{10} filters was measured at the paleomagnetic laboratory of Istituto Nazionale di Geofisica e Vulcanologia using a AGICO KLY-5 meter with a plastic vessel suitable for containing unfolded filters.

Under the assumption of an arbitrary volume of 10 cm^3, the nominal volume of the pick-up coils, the volume magnetic susceptibility of daily filters (k) was computed as the average of the last three measurements from a sequence of seven to ten, which were performed to compensate the drift due to static electric charge of the large surface area of the plastic vessel; the correction for the empty vessel was done including an empty glass fiber filter, so that the magnetic susceptibility values were referred to PM_{10} only.

The daily mass of PM_{10} accumulated in each filter was computed multiplying the daily air volume pumped by the stations (55 m^3/day) for the daily PM_{10} concentration; thus, the mass-normalized susceptibility (χ, m^3/kg) was determined as:

$$\chi = (\mathrm{Vo} \times \ \mathrm{k})/\mathrm{m}$$

where:

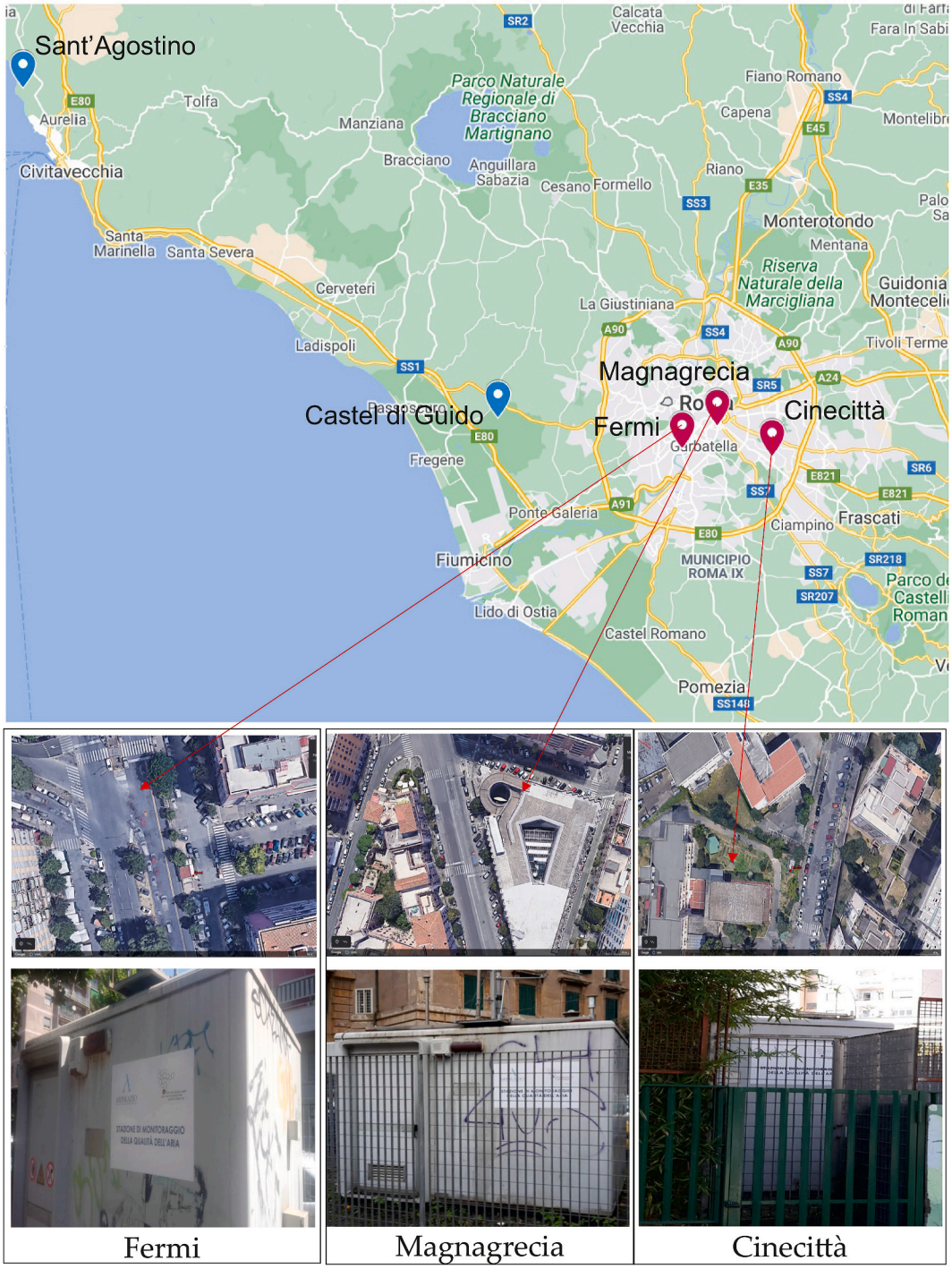

Fig. 1. Localization and photos of the investigated PM_{10} stations: the map and the aerial photos are modified after Google Maps and Google Earth geo-visualizations.

Vo = nominal measuring volume, 10 cm^3
m = daily weight of PM_{10}

The coercive force (B_c), the saturation remanent magnetization by mass (M_{rs} or SIRM) and the saturation magnetization by mass (M_s) were measured on gel caps containing half filter, using a vibrating sample magnetometer (Micromag 3900, PMC) cycling in a maximum field of 1.0 T; concentration dependent hysteresis parameters were calculated after subtracting the high field paramagnetic linear trend and dividing the magnetic moments for ½ m, visually checking uniform dust deposition over the filters. The coercivity of remanence (B_{cr}) values were extrapolated from the backfield curves.

The domain state and magnetic grain-size of the samples were compared to theoretical magnetite according to the hysteresis ratios M_{rs}/M_s vs. B_{cr}/B_c in the "Day plot" (Day et al., 1977, Dunlop, 2002a,b), which is commonly used for deducing the mean domain state of a sample with respect to the single domain (SD), pseudosingle domain (PSD), and multidomain (MD) zones therein demarcated.

First order reversal curves (FORCs, Pike et al., 1999; Roberts et al., 2000) were measured using the Lakeshore 8604 VSM; FORC diagrams were processed and smoothed with the FORCINEL 3.05 Igor Pro routine (Harrison and Feinberg, 2008), with FORCs measured in steps of 2.5 mT up to 1.0 T, 300 ms averaging time and smoothing factors 3 or 4.

FORC diagrams provide information regarding magnetic reversal

mechanisms in ferromagnetic minerals: they are used for delineating the distributions of the interaction field (B_u) and coercivity in samples and to distinguish between SD, MD and PSD behaviors, the latter recently referred as "vortex state" for better describing the transitional state between SD and MD.

Statistical data analysis was performed with Microsoft Excel and Past 4.05 free software (Hammer et al., 2001).

3. Results

3.1. An overview of traffic and PM_{10} concentration data during the lockdown

Vehicular traffic, in terms of cars/month and cars/hour, is reported in Fig. 2a and b for the main roads of the same ~S-E Rome quadrant where the analyzed urban PM_{10} stations are located: traffic data were provided by Rome Municipality at https://romamobilita.it/it/covid-19-impatto-sulla-mobilita; the percentage variation of transit mobility in Rome was elaborated in Fig. 2c with data provided by Apple (https://covid19.apple.com/mobility) and following Chapin and Roy (2021): the traffic variations were referred to the pre-lockdown 13 January 2020 level.

According to Gualtieri et al. (2020), the road mobility in Rome varied between −5 and −94% with respect to 2019 in the period 24/02/2020 to 30/04/2020, overall averaging −52% with a median decrease of 65% and in general agreement with mobile phone data analyzed by the Swiss company Teralytics, who provided a similar value (−61%) for the period 23/02/2020 to 27/03/2020 for the Italian newspaper "La Repubblica"(https://lab.gedidigital.it/repubblica/2020/cronaca/coronavirus-mappa-italia-impatto-sulla-mobilita/).

For a comparison, ANAS, the Italian national road board, distinguished between light and heavy vehicular transportation to provide the national mobility index shown in Fig. 2d, modified after Amoroso et al. (2020).

Independently of the data supplier, a sharp drop of vehicular traffic, up to −78% in April with respect to February, was evident in Rome during the lockdown; soon after the end of the strictest measures, a prompt raise up to the pre-lockdown levels followed, with short term drops during the Christmas and Easter holidays, when rigorous limitations were active again.

The weather conditions in Rome during the lockdown are summarized in Supplementary Text 1, abridged from the comprehensive description by Amoroso et al. (2020), who reported, for the whole period, low rainfalls and winds, with two main Saharian and/or Caucasic dusts transportation events occurring from 26 to 30 March and from 13 to 18 May 2020.

Amoroso et al. (2020) compiled an extensive analysis of PM_{10} concentration data: in Rome metropolitan area, from March to May, a moderate decrease with respect to the previous years was evident in April only, and was not comparable to what was estimated for NO_2 (−47%), NO and C_6H_6 (>60%) (Fig. 1s a, b, c, d, respectively).

The average monthly PM_{10} concentrations for the stations located inside the GRA of Rome, as well as the suburban background values of Castel di Guido are reported in Table 1s, computed for the years 2016–2020.

The monthly statistics (mean, median, 25th and 75th percentiles) of PM_{10} concentration at Fermi for March, April and May for years 2016–2020 is reported in Table 2s: in March 2020, there was a slight decrease for the above mentioned statistical parameters, that was more marked in April and May 2020, with respect to the previous years.

Overall in Rome, during March and April, the PM_{10} concentration levels in traffic areas approached those measured at rural contexts close to the city, with an average reduction, compared to the last four years, estimated at about 9% for the stations inside the GRA; the concentration decrease was uneven and station specific in May (Fig. 1s a).

3.2. PM_{10}, k and χ values during and after the lockdown

PM_{10} concentration, k, χ, M_s, M_{rs}, B_c and B_{cr} minimum, maximum, mean values and standard deviations (sd) are reported in Table 1, computed separately for the whole period, during and after the lockdown; the hysteresis parameters were discarded at Sant'Agostino, due to their unreliable values for the low concentration of magnetic minerals.

The bar-charts of PM_{10} concentrations, k and χ values, during and after the lockdown, are shown in Fig. 3: according to One-Way ANOVA or Kruskal-Wallis tests, the latter adopted for variables not normally distributed, there was no significant difference at 95% confidence level between PM_{10} concentration variances or medians during and after lockdown for all the stations but Cinecittà (Fig. 3d), where PM_{10} levels significantly decreased.

Fermi and Magnagrecia showed the highest average values of k and χ, $1.28 \pm 0.67 \times 10^{-6}$ SI, $12.90 \pm 5.75 \times 10^{-6}$ m^3/kg and $1.86 \pm 1.30 \times 10^{-6}$ SI, $15.00 \pm 8.32 \times 10^{-6}$ m^3/kg, respectively and for the whole period (Table 1), with k and χ medians significantly increasing after the lockdown (Fig. 3 b,c and h,i, respectively).

Cinecittà followed, with average $k = 0.44 \pm 0.26 \times 10^{-6}$ SI and $\chi = 4.07 \pm 2.58 \times 10^{-6}$ m^3/kg for the whole period (Table 1), and no significant changes for volume and mass susceptibilities after the lockdown (Fig. 3 e, f).

At the suburban and rural background stations, $k = 0.13 \pm 0.08 \times 10^{-6}$ SI and $0.08 \pm 0.07 \times 10^{-6}$ SI, $\chi = 1.25 \pm 0.83 \times 10^{-6}$ m^3/kg and 1.05 ± 0.97 10^{-6} m^3/kg were the average magnetic susceptibility values for Castel di Guido and Sant'Agostino, respectively.

In Castel di Guido, both magnetic susceptibilities significantly increased after the lockdown, while in Sant'Agostino no parameter statistically changed (Fig. 3 m, n and p, q); the summary statistics of One-way ANOVA or Kruskal-Wallis tests is reported in Table 3s.

3.3. PM_{10} concentration vs volume and mass magnetic susceptibilities

The linear correlation between PM_{10} concentrations, χ and k was tested during and after the lockdown: in Fermi (Fig. 4a), during the lockdown, there was no correlation between PM_{10} concentrations and k ($R^2 = 0.00$), while the correlation became significant after the lockdown ($R^2 = 0.60$). By contrast, χ negatively correlated with PM_{10} during the lockdown ($R = -0.56$), switching to no correlation ($R^2 = 0.01$) afterwards (Fig. 4b).

Magnagrecia behaved accordingly, with R^2 (PM_{10} vs k) changing from 0.00 to 0.73 after the lockdown, and a significant negative correlation between χ and PM_{10} ($R = -0.56$) decreasing to $R = -0.33$ after the lockdown (Fig. 4 e, f).

The linear model was opposite in Cinecittà station, with R^2 (PM_{10} *vs* k) decreasing from 0.42 to 0.14 after the lockdown, and R^2 (PM_{10} *vs* χ) decreasing from 0.07 to 0.00 (Fig. 4 c, d).

In Castel di Guido (Fig. 4 g, h), R^2 (PM_{10} *vs* k) decreased from 0.28 to 0.01 after the lockdown and R^2 (χ vs PM_{10}) changed from 0.00 to 0.21 (significant negative correlation, $R = -0.46$); in Sant'Agostino, the variations after the lockdown were negligible, with R^2 changing from 0.19 to 0.12 and from 0.00 to 0.04 for k and χ, respectively.

The daily trends of PM_{10} concentration and χ are shown in Fig. 5; the values were normalized to their whole period means, in analogy with Sagnotti et al. (2006) and for avoiding flat diagrams around peaks: a straightforward temporal relationship between PM_{10} and χ did not emerge in any series; conversely, anticorrelated points, that is χ minima on the same dates of PM_{10} maxima, were evident during exogenous dusts atmospheric events.

3.4. Hysteresis properties

The hysteresis properties were analyzed on selected filters, regularly spaced between the samples chosen for peculiar PM_{10} concentrations or susceptibility values: 14 and 8 samples were analyzed for Fermi, 12 and

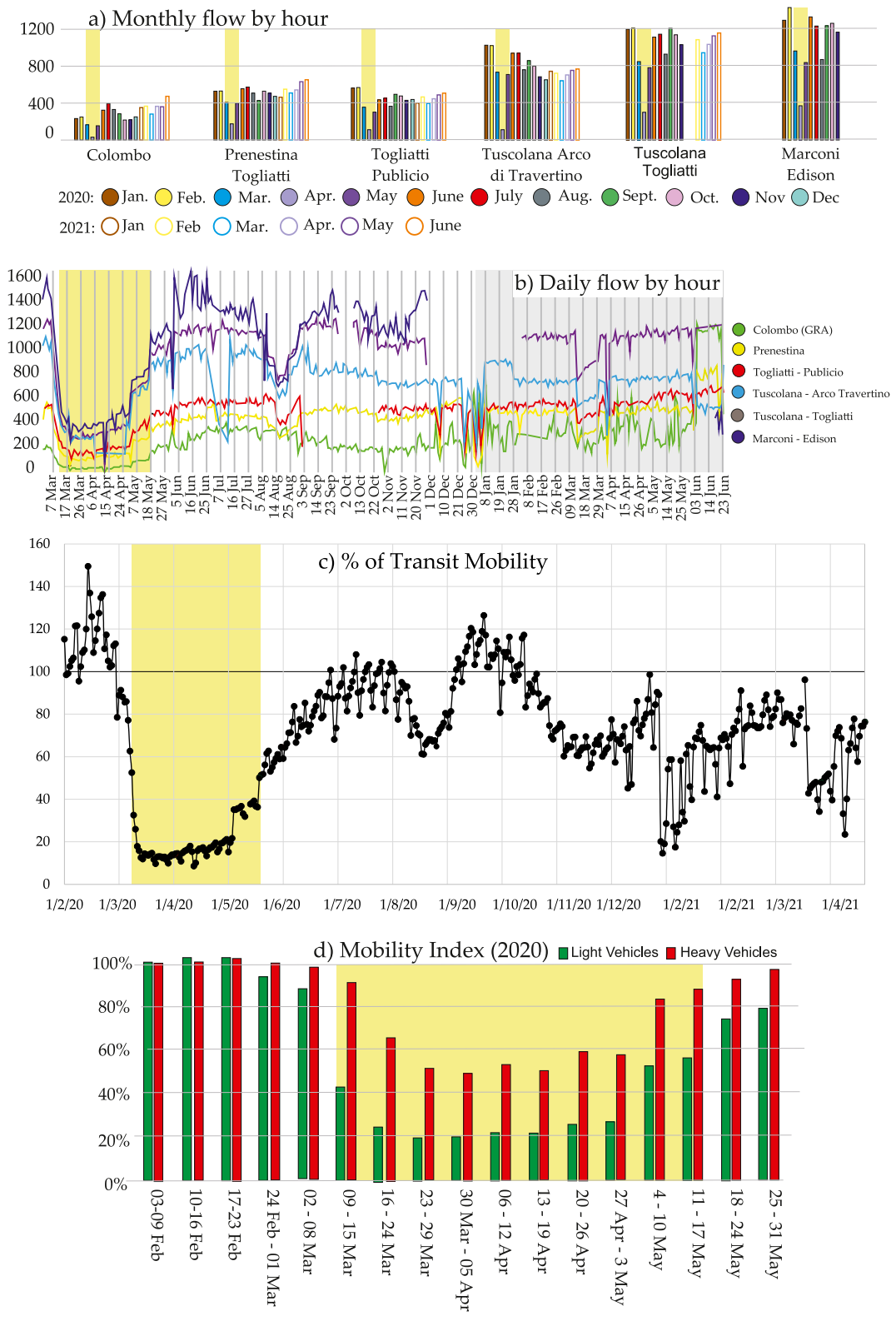

Fig. 2. Daily (a) and monthly (b) traffic flows by hour recorded in a ~S-E quadrant of Rome, for roads with different traffic volumes (modified from Rome Municipality website; 2021 data in grey background). (c) Percentage variation of transit mobility referred to 13 January 2020 in Rome; data by Apple; short intervals of traffic drops were recorded during the containment measures of Christmas and Easter holidays. (d) national Mobility Index normalized to the first week of February 2020, computed for light and heavy vehicles by ANAS, the Italian national road board. Independently of the data supplier, a sharp drop of vehicular traffic was evident during the lockdown, followed by a prompt raise up to the pre-lockdown levels immediately afterwards. Lockdown data are in yellow background.

Table 1
Minimum, maximum, average and standard deviation values for PM_{10} concentration, volume magnetic susceptibility (k), mass magnetic susceptibility (χ) and hysteresis parameters M_s, M_{rs}, B_c and B_{cr}. Data were computed for the whole period, during and after the lockdown: the sampling intervals are station specific and are reported in paragraph 2.1. Hysteresis parameters were not available (N/A) in Sant'Agostino for the weak magnetic properties.

	PM_{10} (min, max, mean, sd) $\mu g/m^3$	k (min, max, mean, sd) 10^{-6} SI	χ (min, max, mean, sd) 10^{-6} m^3/kg	M_s (min, max, mean, sd) Am^2/kg	M_{rs} (min, max, mean, sd) 10^{-1} Am^2/kg	B_c (min, max, mean, sd) mT	B_{cr} (min, max, mean, sd) mT
Fermi whole period	7.0	0.35	1.17	0.25	0.17	5.1	41.3
	74.0	3.34	33.60	2.53	1.64	9.4	51.0
	19.9	1.28	12.90	1.09	0.80	7.1	47.2
	10.2	0.67	5.75	0.53	0.35	1.1	2.4
Fermi lockdown	7.0	0.35	1.17	0.25	0.17	5.1	41.3
	74.0	2.27	33.60	2.53	1.64	9.4	51.0
	21.0	0.93	9.96	1.00	0.73	7.1	47.7
	12.5	0.39	5.78	0.58	0.37	1.0	2.5
Fermi after lockdown	8.0	0.56	7.39	0.58	0.53	5.8	42.7
	41.0	3.34	25.90	1.90	1.42	9.3	50.2
	18.9	1.59	15.60	1.25	0.93	7.2	46.4
	7.7	0.72	4.31	0.47	0.32	1.4	2.3
Cinecittà whole period	9.0	0.01	0.22	0.10	0.09	4.9	32.0
	57.0	0.99	12.90	1.15	1.27	11.8	51.7
	21.2	0.44	4.07	0.44	0.44	9.0	43.2
	10.8	0.26	2.58	0.27	0.29	1.8	4.9
Cinecittà lockdown	9.0	0.11	1.50	0.10	0.09	4.9	32.0
	57.0	0.99	12.90	1.15	1.27	10.5	49.5
	24.1	0.47	3.83	0.38	0.40	8.7	41.3
	12.6	0.25	2.28	0.30	0.34	1.9	4.5
Cinecittà after lockdown	10.0	0.01	0.22	0.29	0.33	6.9	43.7
	25.0	0.88	12.20	0.69	0.67	11.8	51.7
	16.5	0.39	4.33	0.55	0.52	9.4	47.2
	3.9	0.26	3.10	0.17	0.14	1.9	3.3
Magnagrecia whole period	5.0	0.45	1.69	0.17	0.14	5.2	43.1
	73.0	6.50	51.40	3.15	2.49	9.5	51.6
	24.8	1.86	15.00	1.34	0.97	7.0	46.8
	14.4	1.30	8.32	0.78	0.57	1.2	2.3
Magnagrecia lockdown	8.0	0.45	1.69	0.17	0.14	5.8	43.1
	73.0	1.80	29.70	3.02	2.49	9.4	51.6
	23.3	1.03	9.67	0.99	0.79	7.6	47.6
	12.6	0.35	5.40	0.74	0.61	1.1	2.7
Magnagrecia after lockdown	5.0	0.60	7.35	0.50	0.27	5.2	43.8
	70.0	6.50	51.40	3.15	2.08	9.5	49.8
	26.0	2.50	19.10	1.66	1.13	6.5	46.0
	15.8	1.41	7.95	0.74	0.53	1.1	1.72
Castel Di Guido whole period	8.00	−0.04	−0.78	0.04	0.06	8.1	38.6
	67.00	0.33	4.22	0.29	0.51	21.5	59.9
	19.62	0.13	1.25	0.18	0.25	14.5	49.5
	10.40	0.08	0.83	0.08	0.16	4.3	6.0
Castel Di Guido lockdown	8.00	−0.04	−0.78	0.04	0.06	15.5	38.6
	67.00	0.28	2.23	0.28	0.51	21.5	49.9
	21.66	0.11	0.93	0.15	0.26	18.3	46.0
	12.44	0.08	0.59	0.09	0.13	2.4	4.4
Castel Di Guido after lockdown	10.00	0.04	0.41	0.11	0.09	8.1	44.8
	25.00	0.33	4.22	0.29	0.31	13.5	59.9
	16.07	0.15	1.79	0.21	0.23	10.7	53.1
	3.62	0.07	0.93	0.07	0.09	2.5	6.5
Sant'Agostino whole period	2.0	−0.02	−0.28	N/A	N/A	N/A	N/A
	50.0	0.39	4.80				
	15.0	0.08	1.05				
	8.4	0.07	0.97				
Sant'Agostino lockdown	2.0	−0.02	−0.28	N/A	N/A	N/A	N/A
	50.0	0.38	4.80				
	15.9	0.09	1.05				
	9.3	0.09	1.07				
Sant'Agostino after lockdown	6.0	0.00	0.13	N/A	N/A	N/A	N/A
	26.0	0.03	3.89				
	13.3	0.07	1.05				
	5.5	0.05	0.74				

5 for Cinecittà, 12 and 13 for Magnagrecia, 5 and 5 for Castel di Guido, during and after the lockdown, respectively. In Sant'Agostino, it was not possible to obtain reliable hysteresis parameters due to the low concentration of magnetic minerals.

All the hysteresis loops were similar in shape, saturated well before 1T and usually narrow, except at Castel di Guido, where B_c values were on average higher (Table 1).

Magnetite-like minerals were the main magnetic carriers, as confirmed by SIRM/χ values (Thompson and Oldfield, 1986) which, on average for the whole period, were very close for Fermi and Magnagrecia (6120 ± 941 A/m and 6781 ± 1712 A/m, respectively), and higher at Cinecittà (9084 ± 1235 A/m). At Castel di Guido, SIRM/χ values were on average 13049 ± 5774 A/m, with a large decrease after the lockdown; the average SIRM/χ values during and after the lockdown are reported in Table 4s.

The relatively high values of B_{cr}, with respect to pure magnetite,

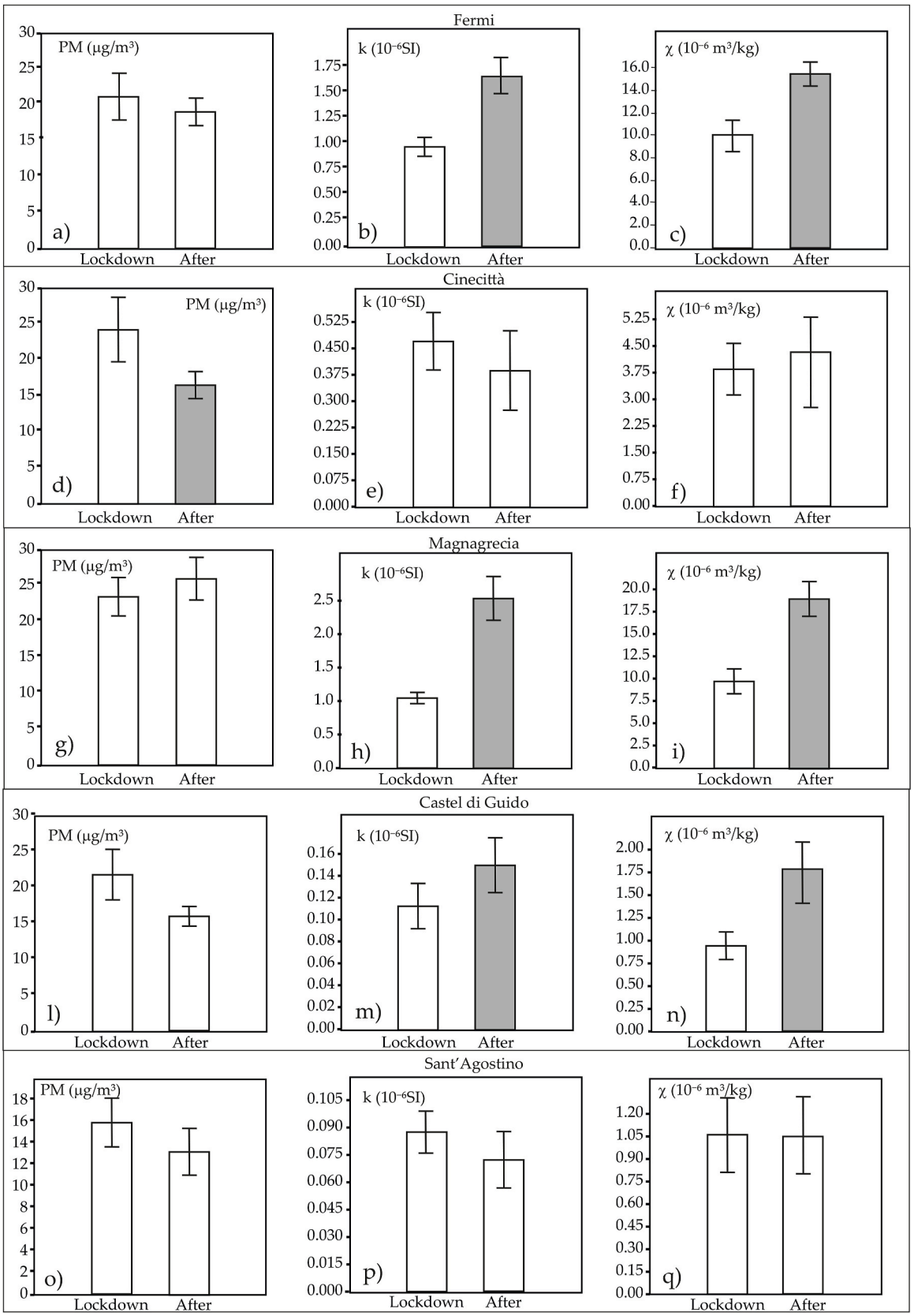

Fig. 3. Bar-charts of PM_{10} concentration, volume susceptibility (k) and mass susceptibility (χ) during and after the lockdown. The length of the standard error bars is the 95% confidence interval. Bars of the same color indicate no significant difference at 95% during and after the lockdown, according to the Kruskal-Wallis or one-way ANOVA tests on medians or variances; see text for discussion.

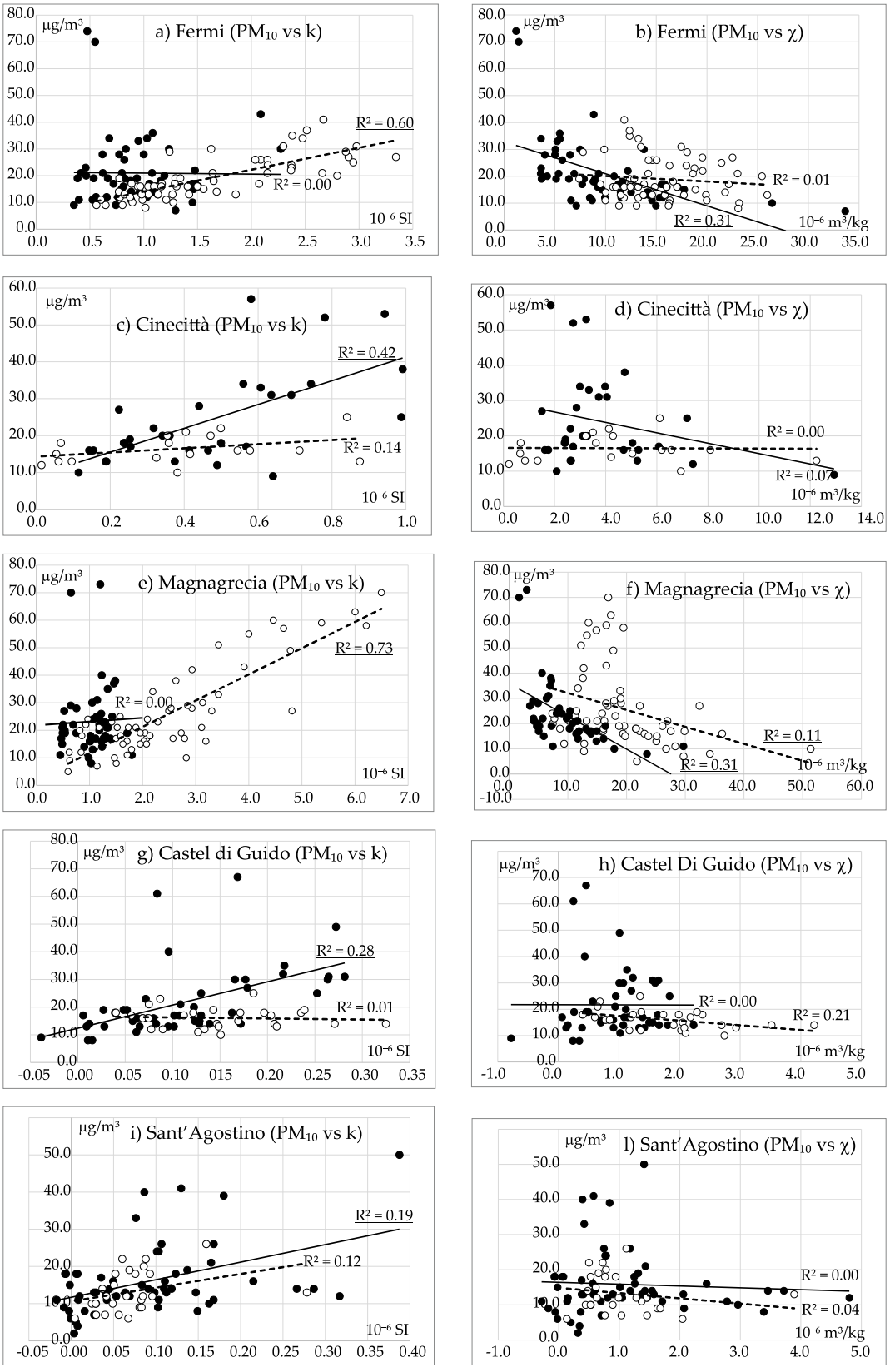

Fig. 4. Linear models between PM_{10} concentration and volume (k) or mass (χ) susceptibility. Black and white circles represent lockdown and after lockdown data, respectively. The linear regressions are represented with continuous lines during the lockdown, dashed afterwards; R^2 is underlined for significant correlation at 95% confidence level; see the text for discussion.

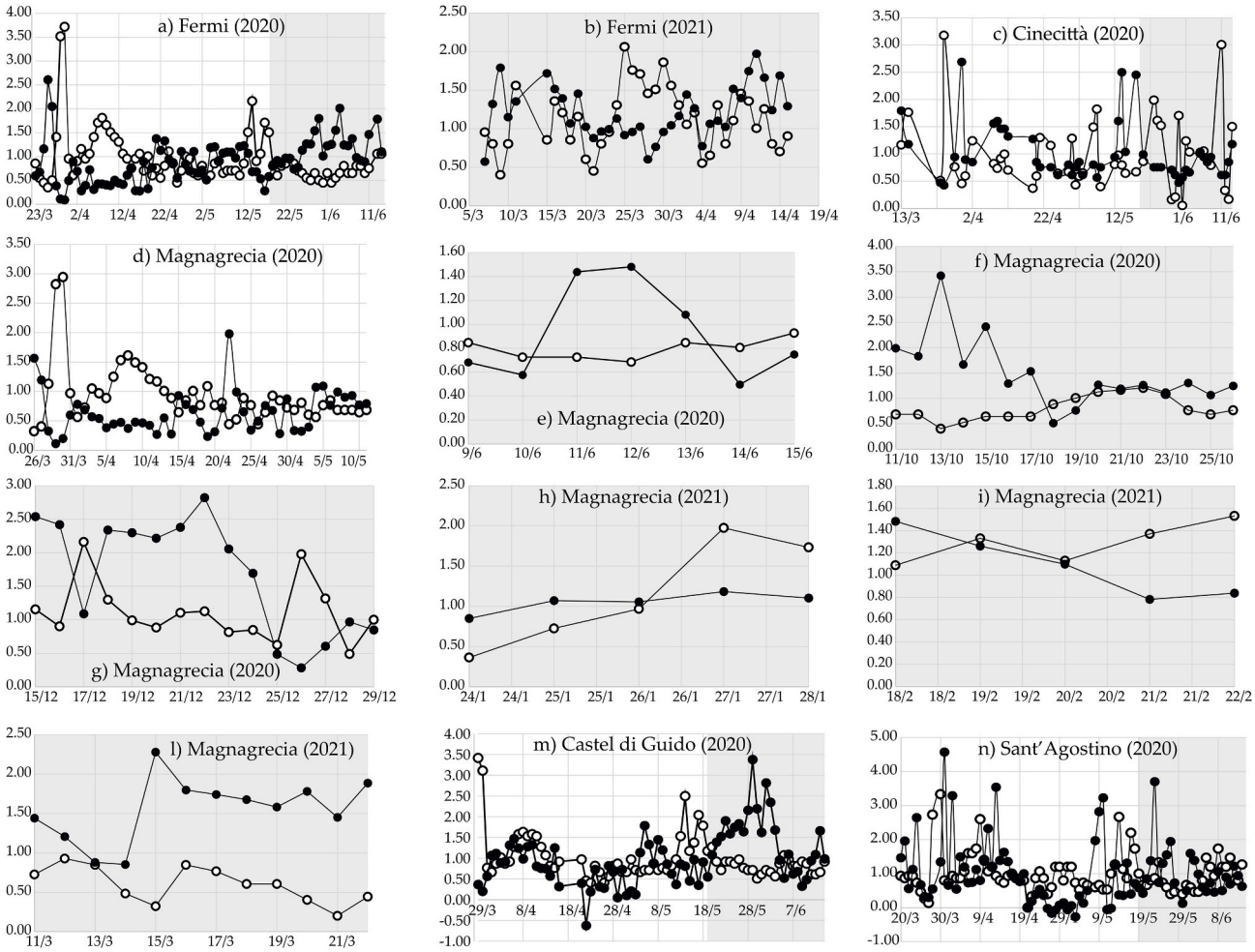

Fig. 5. Daily trends of PM_{10} concentrations (white symbols) and mass susceptibility (χ, black symbols): values were normalized to their means for the whole period. Data after lockdown are in grey background; see the text for discussion.

suggested the presence of a minor higher coercivity ferromagnetic component possibly linked to the presence of oxidized magnetite, maghemite or hematite; see Sagnotti et al. (2006) and Gonet et al. (2021b).

M_s linearly correlated with χ during and after the lockdown, indicating that magnetic susceptibility, whose value are also influenced by the dia and paramagnetic fractions of PM, was primarily carried by the magnetic minerals: in particular, R^2 was 0.92, 0.99 and 0.91 for Fermi, Cinecittà and Magnegrecia, respectively, with no substantial variations during and after the lockdown; in Castel di Guido, R^2 (χ vs M_s) = 0.61, as a consequence of the lower concentration of magnetic minerals.

Upon the assumption that magnetite-like minerals dominated the magnetic mineralogy of the filters, the magnetite weight percentage fraction wt%, with respect to the total mass of PM_{10}, was calculated dividing M_s for the saturation magnetization of magnetite, $J_s = 90\ Am^2/kg$; the minimum, maximum and average values of wt% are reported in Table 2.

In the "Day Plot", the M_{rs}/M_s vs. B_{cr}/B_c site mean ratios (Fig. 6) indicated that the filters from Fermi and Magnagrecia were placed in the middle-right side of the plot both during and after the lockdown, between the theoretical curves calculated for mixtures of single domain (SD) and multidomain (MD) magnetite grains and that calculated for a mixture of SD and superparamagnetic (SP) particles (Dunlop, 2002a,b); the Day Plot of individual samples is in Fig. 1s.

During and after the lockdown the points for Cinecittà approached the PSD central zone of the plot, while the Castel di Guido lockdown site mean fell in the upper side of the plot, near the theoretical trends for equal proportions of SD and MD magnetite.

After the lockdown, the Castel di Guido point overlapped the Cinecittà points.

A selection of FORC diagrams and horizontal coercivity distributions from urban traffic and suburban background stations is shown in Fig. 7: except Castel di Guido, MD features prevailed, with open contours diverging towards the vertical magnetic interactions B_u axis and the distribution peaking at the origin of the diagram. The presence of secondary vortex/PSD features was nevertheless suggested by a feebly developed ridge at 135° for negative values of B_u.

During the exogenous dusts atmospheric event of 29 March 2020, the FORC distribution of Castel di Guido highlighted a SD component centered around 20 mT, influencing also the coercivity distribution of

Table 2
Minimum, maximum and average weight percentage fraction (wt%) of magnetite-like minerals with respect to the total mass of PM_{10}, evaluated during and after the lockdown; (*): neglecting an outlier.

	Fermi wt %	Cinecittà wt%	Magnagrecia wt%	Castel di Guido wt%
Min, Max, Average Lockdown	0.3, 2.8, 1.1 (03, 1.6, 0.9) *	0.1, 1.3, 0.4	0.2, 3.4, 1.1	0.04, 0.31, 0.17
Min, Max, Average After Lockdown	0.6, 2.1, 1.4	0.3, 0.8, 0.6	0.6, 3.5, 1.8	0.12, 0.33, 0.23

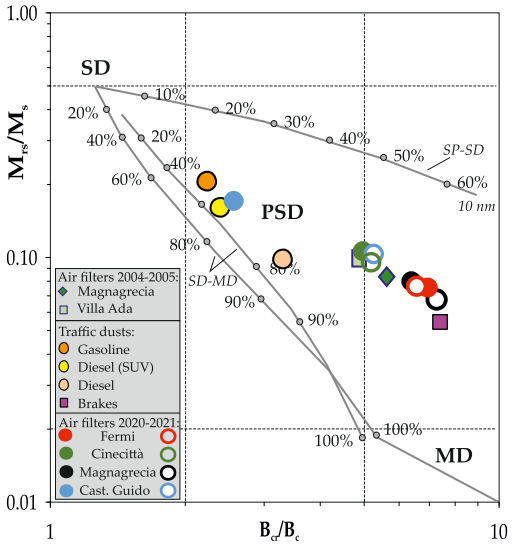

Fig. 6. Bilogarithmic Day plot of the hysteresis ratios M_{rs}/M_s vs. B_{cr}/B_c for Fermi (red), Cinecittà (green), Magnagrecia (black) and Castel di Guido (blue), averaged at station level. Closed circles are during lockdown, open circles afterwards. Also reported: mean values for air filters from monitoring stations in Rome (green diamonds and squares), fuel exhausts (orange, yellow and pink dots) and brake dusts (purple squares), calculated after Sagnotti et al. (2006) and Sagnotti et al. (2009). The SD (single domain), PSD (pseudo-single domain) and MD (multidomain) fields and the theoretical mixing trends for SD-MD and SP-SD pure magnetite particles (SP, superparamagnetic) are from Dunlop (2002a,b). Fermi and Magnagrecia points were located, during and after the lockdown, near "brakes"; Cinecittà (both periods) and Castel di Guido (after lockdown) fell near the urban background in Sagnotti et al. (2006). Castel di Guido, during the lockdown, was in the upper zone of the plot, near to fuel emissions and fine natural magnetite.

Magnagrecia on the same day (Fig. 7 a, f, g, n).

4. Discussion

4.1. Urban traffic stations: Fermi and Magnagrecia

Fermi and Magnagrecia stations, located in urban traffic contexts, showed robust similarities, useful for the characterization of vehicular magnetic emissions and for recognizing the impact of the lockdown measures on the variations of the magnetic properties of PM_{10} filters.

PM_{10} concentrations did not show a significant difference during and after the lockdown, at 95% confidence level (Fig. 3a, g).

During the lockdown, both stations recorded persistent high concentration of magnetic particles, as deduced from the intense magnetic susceptibility and M_s values (Table 1).

For a comparison, the average values of k and χ during the lockdown ($0.93 \pm 0.39 \times 10^{-6}$ SI and $996 \pm 578 \times 10^{-8}$ m^3/kg for Fermi and $1.03 \pm 0.35 \times 10^{-6}$ SI and $967 \pm 540 \times 10^{-8}$ m^3/kg for Magnagrecia) were about the half of what was measured in Sagnotti et al. (2006) at Magnagrecia station from July 2004 to July 2005 ($2.06 \pm 0.72 \times 10^{-6}$ SI and $2117 \pm 619 \times 10^{-8}$ m^3/kg for k and χ, respectively).

After the lockdown, k and χ significantly increased (Fig. 3b, c, h, i) to the average values $1.59 \pm 0.72 \times 10^{-6}$ SI; $1560 \pm 431 \times 10^{-8}$ m^3/kg for Fermi and $2.50 \pm 1.41 \times 10^{-6}$ SI; $1910 \pm 795 \times 10^{-8}$ m^3/kg for Magnagrecia, approaching or even overtaking those in Sagnotti et al. (2006) and empirically well representing the >50% traffic increase after the lockdown (Fig. 2).

The linear correlation k vs PM_{10} changed between lockdown and after lockdown, switching from no correlation ($p = 0.93$ and $p = 0.80$) to significant correlation ($p < 0.01$) for Fermi and Magnagrecia, respectively (Fig. 4b, f).

In Fermi, two different correlation regimes were evident for χ vs PM_{10} too, switching from negative during the lockdown ($p < 0.01$) to no correlation ($p = 0.37$) afterwards; in Magnagrecia, R^2 decreased threefolds after the lockdown (Fig. 4c, g).

The daily trends of PM_{10} concentration and χ (Fig. 5) showed no prolonged time-intervals where χ was constant, that is k varying as PM_{10} concentration; only in Magnagrecia, after the lockdown, χ values were approximately uniform for PM_{10} concentration >35 μg/m^3 (Fig. 4f), implying a rather constant magnetic fraction inside filters.

PM_{10} concentration frequently increased more than k: in this case, χ minima were associated to a relative increase of the nonmagnetic fraction of PM_{10}, especially during inputs of exogenous atmospheric dusts (26–30 March 2020, Fig. 5a, c, d, m).

When PM_{10} concentration decreased more (or increased less) than k (eg. Fermi, June 2020, Fig. 5b), χ maxima were associated to increased proportions of magnetic PM inside the filters.

During the lockdown, at traffic stations, the variations of PM_{10} concentration were not linked to the traffic-related magnetic fraction; therefore, the variation of PM_{10} concentrations were mainly related to natural sources, including exogenous dust transportation events. The persisting high values of k and χ were attributed to resuspension and accumulation of traffic related particles in absence of main rain and wind events (Supplementary Text 1).

After the lockdown, k significantly represented PM_{10} concentration: thus, their mutual variations were connected to the restored levels of vehicular traffic, with Christmas and Easter short-term containments not affecting their correlation.

Concerning the quantification of magnetite-like minerals, their wt% values for Fermi and Magnagrecia (Table 2) were considerably higher with respect to those estimated in trafficked roadside dust from Lancaster (between ~0.18 and 0.63 wt%) and Birmingham (~0.32–0.95 wt %), thus highlighting intense and alarming emissions of harmful anthropic particles (Maher et al., 2016; Hammond et al., 2021; Calderón-Garcidueñas et al., 2019).

In Magnagrecia, the wt% of magnetite spanned from 0.2 to 3.5%, implying that extreme changes in traffic-related magnetic emissions may be masked by a variation of less than a single digit in PM_{10} concentration levels: PM_{10} concentration data alone did not efficiently recorded the major traffic increase after the end of the lockdown, which was properly interpreted by means of complementary magnetic analyses.

4.2. Low traffic and backgrounds stations: Cinecittà, Castel di Guido and Sant'Agostino

In Cinecittà station, the average k and χ values ($0.47 \pm 0.25 \times 10^{-6}$ SI and $383 \pm 228 \times 10^{-8}$ m^3/kg, respectively) were considerably lower with respect to Fermi and Magnagrecia, reflecting the different urban setting (Table 1).

These values were even lower than those recorded in Villa Ada urban background station in 2004–2005 (Sagnotti et al., 2006) and afterwards interpreted in Fusaro et al. (2021), who found relatively high magnetic susceptibility values on the leaves sampled near the entrance of the Villa, in correspondence to a busy road.

Lower magnetic susceptibility values were measured at the suburban background station of Castel di Guido and at the rural background of Sant'Agostino, where average k and χ values dropped to $0.13 \pm 0.08 \times 10^{-6}$ SI; $125 \pm 83 \times 10^{-8}$ m^3/kg and $0.08 \pm 0.07 \times 10^{-6}$ SI; $105 \pm 97 \times 10^{-8}$ m^3/kg, respectively, with k lower than the Fontechiari regional rural background in Sagnotti et al. (2006).

Cinecittà and Sant'Agostino showed no significant difference during and after the lockdown for k and χ (Fig. 3 e, f), with PM_{10} concentration significantly decreasing in Cinecittà station after the lockdown (Fig. 3d).

Castel di Guido showed a significant increase of k and χ after the lockdown (Fig. 3 m, n), under unsignificant variations of PM_{10} concentration (Fig. 3l); in this sense, Sant'Agostino constituted the most

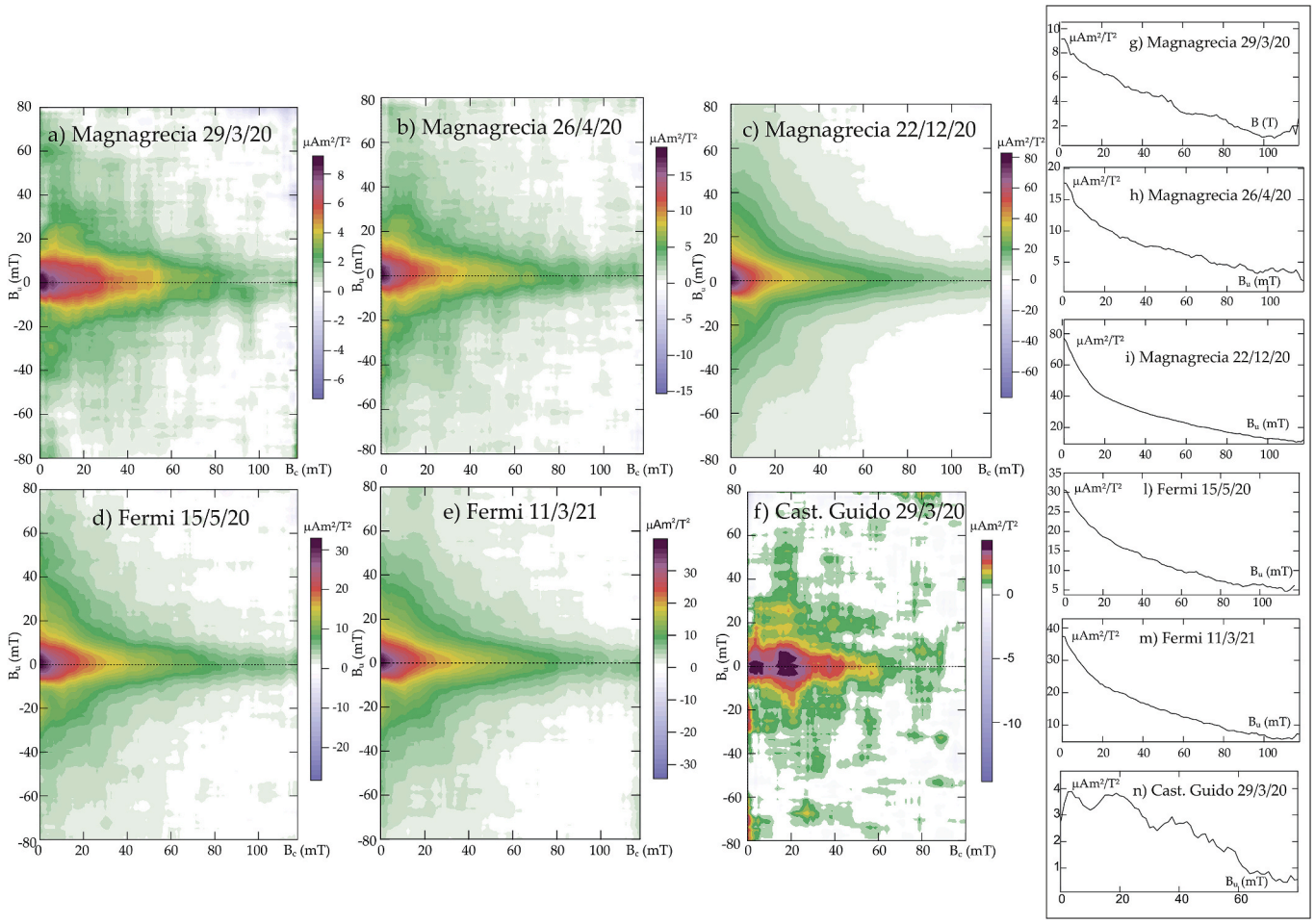

Fig. 7. FORC diagrams and horizontal coercivity (B_c) distributions for selected filters: Magnagrecia (a, g) and Castel di Guido (f, n) during the exogenous dusts atmospheric event of 29 March 2020; Magnagrecia (b, h) during and after (c, i) the lockdown; Fermi during (d, l; Saharian event) and after the lockdown (e, m). Except Castel di Guido, multidomain (MD) features prevailed for all the samples, with secondary vortex traits suggested by the weak ridge at 135° for negative values of B_u, the magnetic interaction field. In Castel di Guido, 29 March 2020, the FORC distribution showed SD features centered around 20 mT, influencing the coercivity distribution of Magnagrecia on the same date (g, n).

proper background station, being completely unaffected by the lockdown (Fig. 3 o, p, q).

In Cinecittà, the linear regressions between k and χ vs PM_{10} were different with respect to the traffic urban stations, with a significant correlation between k and PM_{10} ($p < 0.01$) during the lockdown switching to no correlation ($p = 0.12$) thereafter (Fig. 4c); PM_{10} and χ did not correlate (Fig. 4d) during ($p = 0.18$) and after the lockdown ($p = 0.95$).

In Castel di Guido, there was a significant correlation between k and PM_{10} ($p < 0.01$) during the lockdown, switching to no correlation ($p = 0.71$) thereafter (Fig. 4g); PM_{10} and χ (Fig. 4h) did not correlate during the lockdown ($p = 0.99$) and negatively correlated after the lockdown ($p = 0.02$).

Finally, Sant'Agostino was the only station where the correlations remained practically unvaried (Fig. 4 i, l, m), confirming that it was substantially uninfluenced by the traffic conditions.

Overall, these results showed that the correlation between k and PM_{10} is site dependent and occur more easily when «end-members» periods occur, that is prevailing clean or heavy polluted conditions. An anticorrelation between PM_{10} concentration and χ emerged during intermediate/mixed conditions, when resuspension and natural sources prevailed in trafficked sites or when traffic emissions increased in cleaner sites.

These results agree with Petrovský et al. (2020), who showed negative correlation between the concentration of iron oxides and PM in atmospheric dust at an industrial site during smoggy period, thus concluding that magnetic monitoring is site specific, reflecting local conditions that determine, at site level, the standard trendlines between the content of iron oxides and pollutants.

The magnetite wt% values in Castel di Guido (Table 2) were compatible with those in Gonet et al. (2021a) for urban background dusts, where magnetite concentration was estimated as ~0.05–0.18 wt % in Lancaster and ~0.05–0.20 wt% in Birmingham.

4.3. *Magnetic mineralogy for the PM_{10} sources analysis*

The role of the "Day Plot" is nowadays under discussion for its intrinsic limitations (Roberts et al., 2018), especially for factors as surface oxidation and magnetic particle mixtures; nevertheless, it was used here as an empirical tool for the comparison with former studies about traffic related magnetic dusts.

In Fig. 6, the PM_{10} filters were compared, at site mean level, to the average points obtained in 2004 and 2005 in Magnagrecia and Villa Ada (Sagnotti et al., 2006), and to fuel and brakes emissions sampled in cars' exhaust pipes and wheel rims (Sagnotti et al., 2009).

The filters from Fermi and Magnagrecia, during and after the lockdown, were very close to the former Magnagrecia and "brake" points, in conformity with the magnetic biomonitoring observations on lichens transplanted in Milan and on leaves sampled in Rome, where multidisciplinary analyses pinpointed brake abrasion as the main source of PM in

urban contexts (Winkler et al., 2020; Fusaro et al., 2021).

The points from Cinecittà, during and after the lockdown, coincided in the central part of the plot, overlapping the urban background of Sagnotti et al. (2006).

The position of Castel di Guido, during the lockdown, was remarkably different, falling in the upper PSD zone of the Day plot and recalling the Fontechiari background area of Sagnotti et al. (2006), that was ascribed to the natural eolian deposits of the northern to mid latitudes; Revuelta et al. (2014), reported that a crustal source of fine magnetic particles was found in Barcelona aerosols too.

After the lockdown, the Castel di Guido filters overlapped the Cinecittà points, thus approaching the moderate urban traffic conditions.

To overcome the "Day Plot" limitations, SIRM/χ, a magnetic grainsize indicator (Table 4s) and FORC diagrams were discussed. The SIRM/χ values for Fermi and Magnagrecia were on average compatible with the brake emissions (6.7 $\pm$ 2.5 kA/m) reviewed in Gonet and Maher (2019) and distinct from gasoline and diesel emissions (13.8 $\pm$ 6.3 kA/m and 14.5 $\pm$ 12.1 kA/m, respectively), with Cinecittà showing a relatively higher SIRM/χ ratio, in the middle between brakes and fuels products.

During the lockdown, Castel di Guido SIRM/χ values were on average much higher (17.2 $\pm$ 5.1 kA/m), suggesting finer magnetic grainsizes, as already highlighted by the higher B_c values (Table 1) and the position in the Day plot: therefore, the main influence of finer natural magnetic particles is suggested; after the lockdown, Castel di Guido SIRM/χ values decreased to the same range of Cinecittà, confirming the Day plot results.

Independently of the lockdown conditions, the FORC distributions of Magnagrecia and Fermi (Fig. 7 b, c, d and e) were peaked at the origin of the diagrams and showed prevailing MD features, with a PSD/vortex secondary component resulting as a weak 135° ridge for negative B_u. On 29 March 2020, during an exogenous dusts atmospheric event, a SD component peaked, at around 20 mT, the noisier FORC distribution of the Castel di Guido filter, and influenced the coercivity distribution of Magnagrecia too (Fig. 7 a, f, g, n).

In Sagnotti et al. (2006) it was concluded that FORC diagrams do not change with main inputs of north African dust; thus, this component might be associated to common natural sources or to a magnetic signature of the Caucasian event occurring between 26 and 30 March: in fact, the FORC diagram and the horizontal distribution of Fermi on 15 May 2020 seem not affected by the Saharian dusts event (Fig. 7d, l).

FORC diagrams closely resembled those for brakes and leaves reported in Sagnotti et al. (2009) and Winkler et al. (2020), in substantial coherence with the considerations made after the Day Plot and SIRM/χ, that is brakes emissions dominate the magnetic properties of PM_{10} in traffic urban contexts, with minor magnetic components related to local or exogenous natural sources, and not excluding exhaust fuel emissions, which might be associated to the 135° ridge.

These results are compliant with Gonet et al. (2021a, 2021b), who concluded that non-exhaust vehicle brake wear is the major source of airborne magnetite; they also estimated that, at the roadside of Lancaster and Birmingham, brake wear contributes between ~68% and 85% of the total airborne magnetite in the roadside environment, followed by diesel exhaust emissions (~7%–12%), petrol exhaust emissions (~2%–4%) and background dust (~6%–10%).

Brake wear debris comprises metal-bearing components, including, besides Fe, heavy metals such as Cu, Sb, Sn, and Ba; in Gonet and Maher (2019) it was shown that Fe-bearing particles arise from the friction between a brake pad and the cast iron disc: at operating temperatures below 200 °C, abrasive processes dominate, and wear particles >1 μm are mostly generated. At higher temperatures (>190 °C), the concentration of nanoparticles (<100 nm) increases by four to six orders of magnitude and constitutes >90% of total brake dusts.

The grainsize distribution of brakes dusts is debated: recently, Gonet et al. (2021b) demonstrated that most brake-wear particles are smaller than 200 nm, and that even the larger brake-wear PM size fractions are dominated by agglomerates of ultrafine grains. Conversely, Muxworthy et al. (2003) and Sagnotti and Winkler (2012) previously concluded that the SP fraction of traffic-related PM may occur as coating of coarse MD particles and is originated by localized stress in the oxidized outer shell surrounding the core of magnetite-like grains; thus, it should not be considered as a direct proxy of the content of ultrafine particles.

As a summary, in Fermi and Magnegrecia traffic stations the concentration of traffic related magnetic PM, mostly ascribed to non-exhaust brake emissions, roughly doubled after the end of the lockdown phase, reaching almost 2 wt% of the total PM_{10}.

These consistent results were achieved despite the intrinsic limitations of this study, which was addressed to representative PM_{10} stations in Rome, discontinuously sampled after the end of the lockdown: future technical developments should be addressed for operating daily magnetic susceptibility measurements inside air quality stations, with the vision of providing standardized and regulated magnetic parameters useful for air quality monitoring.

Moreover, magnetic measurements well discriminate brakes from other magnetic emissions, but fuel exhausts and fine natural magnetic components are someway difficult to be uncoupled; about the magnetic grainsize, its association with domain state is not always straightforward and, for what concerns the harmful ultrafine magnetic particles, they are difficult to be investigated at standard room temperature for their deciduous magnetic properties.

Finally, the correlation between PM_{10} concentration and magnetic susceptibility is site dependent (Sagnotti et al., 2006; Petrovský et al., 2020), making it unproper to expand these local results to a broader scale: notwithstanding, magnetic analyses provide original parameters for the source apportionment of PM_{10}, especially when unsignificant variations of its concentration levels may mask important changes in vehicular metallic emissions.

5. Conclusions

In Rome, despite vehicular traffic on average was more than halved because of the severe lockdown measures adopted to contain the COVID-19 pandemic (9 March – 18 May 2020), the PM_{10} concentration levels were similar to those of the same period in previous years, with a modest reduction mainly recorded in April.

Under the hypothesis that vehicular traffic is the main source of magnetic emissions in traffic urban contexts, it was carried out a detailed study and comparison of the magnetic properties of PM_{10} filters collected during and after the lockdown from automated stations for air quality monitoring, to assess the impact of the COVID-19 containment measures on the traffic-related fraction of particulate matter.

Here, are reported the main findings:

1) In traffic urban sites, the PM_{10} concentrations did not significantly change after the lockdown, when traffic promptly returned to its usual levels; conversely, the average volume and mass magnetic susceptibilities of PM_{10} filters approximately doubled, and the linear correlation between volume magnetic susceptibility and PM_{10} concentration became significant, highlighting the link between PM_{10} concentrations and the increasing levels of traffic-related magnetic emissions.
2) In the moderate traffic urban station and in the rural background site, the magnetic susceptibility of PM_{10} filters was unaffected by the lockdown: in the suburban background site, the volume and mass magnetic susceptibilities of the filters significantly increased after the lockdown.
3) The magnetic mineralogy of PM_{10} filters was dominated by low coercivity magnetite-like minerals arising from non-exhaust brakes emissions; it was supposed a weak influence of fuel exhausts, while natural magnetic sources emerged far from the main roads and in rural contexts, as well as during exogenous dusts atmospheric events.
4) Magnetic susceptibility demonstrated to be a fast and accurate proxy of the traffic related vehicular emission, and applies for having a key

role in the source apportionment of airborne particulate matter in urban areas, especially when it can be diagnostic of important variations in traffic conditions that are not evident from PM_{10} concentration data alone.

Finally, this study highlighted that during a prolonged stop of vehicular emissions, as it was imposed for containing the Covid-19 pandemic, harmful metallic PM may persist near the busiest roads, reaching back to the highest concentration levels soon after the end of the measures: in this sense, after adopting severe rules for limiting exhaust fuel emissions, a significant reduction of brake wear, as the main source of airborne pollutants, is demanded.

CRediT author statement

Conceptualization: AW, AA, ADG. Methodology: AW. Validation: AW, AA, GM. Formal analysis: AW, AA. Investigation: AW, AA, ADG, GM. Writing - Original Draft: AW. Visualization: AW. Supervision: AW, AA, ADG, GM. Funding acquisition: AA, ADG.

Declaration of competing interest

The authors declare that they have no known competing financial interests or personal relationships that could have appeared to influence the work reported in this paper.

Acknowledgement

This study was realized and funded in the framework of the Agreement between ARPA Lazio and INGV for the magnetic characterization of airborne particulate matter.

The Lakeshore 8604 VSM was funded by the Ministry of University and Research, project PON GRINT, code PIR01_00013 – GRINT.

This study was also supported by INGV Project "Pianeta Dinamico" (MIUR, Task A3 – 2021).

The authors are grateful to the Editor Da Chen for handling the paper with care and to the reviewers for providing thoughtful suggestions.

AW would like to thank Leonardo Sagnotti for providing past Magnagrecia data and for the fruitful discussions. AW dedicates this work to his son Lorenzo, in celebration of his Bar Mizvah.

Appendix A. Supplementary data

Supplementary data to this article can be found online at https://doi.org/10.1016/j.envpol.2021.118191.

References

Amoroso, A., Di Giosa, A.D., Ferrario, M.E., Listrani, S., Marchegiani, G., Marinelli, A., Occhiuto, D., 2020. L'effetto sulla qualità dell'aria nel Lazio dell'emergenza COVID-19, Analisi preliminare dei dati (marzo-maggio 2020). http://www.arpalazio.gov.it/download/?sez=eventi&pid=112&fln=Report_QA_COVID_maggio_2020.pdf.

Calderón-Garcidueñas, L., González-maciel, A., Mukherjee, P.S., Reynoso-Robles, R., Pérez-Guillé, B., Gayosso-Chávez, C., Torres-Jardón, R., Cross, J.V., Ahmed, I.A.M., Karloukovski, V.V., et al., 2019. Combustion- and friction derived magnetic air pollution nanoparticles in human hearts. Environ. Res. 176.

Castaneda-Miranda, A.G., Böhnel, H.N., Molina-Garza, R.S., Chaparro, M.A.E., 2014. Magnetic evaluation of TSP-filters for air quality monitoring. Atmos. Environ. 96, 163–174.

Chaparro, M.A.E., Castañeda-Miranda, A.G., Marié, D.C., Gargiulo, J.D., Lavornia, J.M., Natal, M., Böhnel, H.N., 2020. Fine air pollution particles trapped by street tree barks: in situ magnetic biomonitoring. Environ. Pollut. 266 (Pt 1), 115229. https://doi.org/10.1016/j.envpol.2020.115229.

Chapin, C., Roy, S.S., 2021. A spatial web application to explore the interactions between human mobility, government policies, and COVID-19 cases. J geovis spat anal 5, 12. https://doi.org/10.1007/s41651-021-00081-y.

Day, R., Fuller, M., Schmidt, V.A., 1977. Hysteresis properties of titanomagnetites: grain-size and compositional dependence. Phys. Earth Planet. In. 13, 260–267.

Donzelli, G., Cioni, L., Cancellieri, M., Llopis Morales, A., Morales Suárez-Varela, M.M., 2020. The effect of the covid-19 lockdown on air quality in three Italian medium-sized cities. Atmosphere 11, 1118. https://doi.org/10.3390/atmos11101118.

Dunlop, D.J., 2002a. Theory and application of the Day plot (MRS/MS versus HCR/HC) 1. Theoretical curves and tests using titanomagnetite data. J. Geophys. Res. 107.

Dunlop, D.J., 2002b. Theory and application of the Day plot (MRS/MS versus HCR/HC) 2. Application to data for rocks, sediments, and soils. J. Geophys. Res. 107.

EEA and its European Topic Centre on Air Pollution, Noise, Transport and Industrial Pollution, 2020. EEA Report No 9/2020. https://www.eea.europa.eu/publications/air-quality-in-europe-2020-report. report.

Flanders, P.J., 1994. Collection, measurement, and analysis of airborne magnetic particulates from pollution in the environment. J. Appl. Phys. 75, 5931–5936.

Fusaro, L., Salvatori, E., Winkler, A., Frezzini, M.A., De Santis, E., Sagnotti, L., Canepari, S., Manes, F., 2021. Urban trees for biomonitoring atmospheric particulate matter: an integrated approach combining plant functional traits, magnetic and chemical properties. Ecol. Indicat. 126 https://doi.org/10.1016/j.ecolind.2021.107707.

Georgeaud, V.M., Rochette, P., Ambrosi, J.P., Vandamme, D., Williamson, D., 1997. Relationship between heavy metals and magnetic properties in a large polluted catchments: the Etang de Berre (south France). Phys. Chem. Earth 22, 211–214.

Gonet, T., Maher, B.A., 2019. Airborne, vehicle-derived Fe-bearing nanoparticles in the urban environment: a review. Environ. Sci. Technol. 53 (17), 9970–9991. https://doi.org/10.1021/acs.est.9b01505.

Gonet, T., Maher, B.A., Kukutschová, J., 2021a. Source apportionment of magnetite particles in roadside airborne particulate matter. Sci. Total Environ. 752, 141828. https://doi.org/10.1016/j.scitotenv.2020.141828.

Gonet, T., Maher, B.A., Nyirő-Kósa, I., Pósfai, M., Vaculík, M., Kukutschová, J., 2021b. Size-resolved, quantitative evaluation of the magnetic mineralogy of airborne brake-wear particulate emissions. Environ. Pollut. 288, 117808. https://doi.org/10.1016/j.envpol.2021.117808.

Gualtieri, G., Brilli, L., Carotenuto, F., Vagnoli, C., Zaldei, A., Gioli, B., 2020. Quantifying road traffic impact on air quality in urban areas: a Covid19-induced lockdown analysis in Italy. Environ. Pollut. 267, 115682. https://doi.org/10.1016/j.envpol.2020.115682.

Hammer, Ø., Harper, D.A.T., Ryan, P.D., 2001. PAST: paleontological statistics software package for education and data analysis. Palaeontol. Electron. 4 (1), 9pp. http://palaeo-electronica.org/2001_1/past/issue1_01.htm.

Hammond, J., Maher, B.A., Ahmed, I.A.M., et al., 2021. Variation in the concentration and regional distribution of magnetic nanoparticles in human brains, with and without Alzheimer's disease, from the UK. Sci. Rep. 11, 9363. https://doi.org/10.1038/s41598-021-88725-3.

Harrison, R.J., Feinberg, J.M., 2008. FORCinel: an improved algorithm for calculating first-order reversal curve distributions using locally weighted regression smoothing. G-cubed 9.

Hoffmann, V., Knab, M., Appel, E., 1999. Magnetic susceptibility mapping of roadside pollution. J. Geochem. Explor. 66, 313–326.

Hofman, J., Maher, B.A., Muxworthy, A.R., Wuyts, K., Castanheiro, A., Samsonn, R., 2017. Biomagnetic monitoring of atmospheric pollution: a review of magnetic signatures from biological sensors. Environ. Sci. Technol. 51 (12), 6648–6664. https://doi.org/10.1021/acs.est.7b00832.

Hunt, A., Jones, J., Oldfield, F., 1984. Magnetic measurements and heavy metals in atmospheric particulates of anthropogenic origin. Sci. Total Environ. 33, 129–139.

Jordanova, D., Hoffmann, V., Fehr, K.T., 2004. Mineral magnetic characterization of anthropogenic magnetic phases in the Danube river sediments (Bulgarian part) Earth Planet. Sci. Lett. 221 (1–4), 71–89. https://doi.org/10.1016/S0012-821X(04)00074-3.

Kapper, L., Bautista, F., Goguitchaishvili, A., Bógalo, M.F., Cejudo-Ruíz, R., Cervantes Solano, M., 2020. The use and misuse of magnetic methods to monitor environmental pollution in urban areas – Bolet. Sociedad Geológica Mexicana 72 (1). https://doi.org/10.18268/BSGM10.18268/BSGM2020v72n110.18268/BSGM2020v72n1a111219.

Leite, A.d.S., Léon, J.-F., Macouin, M., Rousse, S., Trindade, R.I.F.d., Proietti, A., Drigo, L., Antonio, P.Y.J., Akpo, A.B., Yoboué, V., Liousse, C., 2021. PM2.5 magnetic properties in relation to urban combustion sources in southern west africa. Atmosphere 12, 496. https://doi.org/10.3390/atmos12040496.

Maher, B.A., Ahmed, I.A.M., Karloukovski, V., MacLaren, D.A., Foulds, P.G., Allsop, D., Mann, D.M.A., Torres-Jardòn, R., Calderon-Garciduenas, L., 2016. Magnetite pollution nanoparticles in the human brain. Proc. Natl. Acad. Sci. U.S.A. 113, 10797–10801.

Marié, D.C., Chaparro, M.A.E., Sinito, A.M., 2020. Magnetic biomonitoring of airborne particles using lichen transplants over controlled exposure periods. SN Appl. Sci. 2, 104.

Muxworthy, A.R., Schmidbauer, E., Petersen, N., 2002. Magnetic properties and Mössbauer spectra of urban atmospheric particulate matter: a case study from Munich, Germany. Geophys. J. Int. 150, 558–570.

Muxworthy, A.R., Matzka, J., Davila, A.F., Petersen, N., 2003. Magnetic signature of daily sampled urban atmospheric particles. Atmos. Environ. 37, 4163–4169.

Muxworthy, A.R., Matzka, J., Petersen, N., 2001. Comparison of magnetic parameters of urban atmospheric particulate matter with pollution and meteorological data. Atmos. Environ. 35, 4379–4386.

Putaud, J.-P., Pozzoli, L., Pisoni, E., Martins Dos Santos, S., Lagler, F., Lanzani, G., Dal Santo, U., Colette, A., 2021. Impacts of the COVID-19 lockdown on air pollution at regional and urban background sites in northern Italy. Atmos. Chem. Phys. 21, 7597–7609. https://doi.org/10.5194/acp-21-7597-2021, 2021.

Petrovský, E., Kapička, A., Grison, H., et al., 2020. Negative correlation between concentration of iron oxides and particulate matter in atmospheric dust: case study at industrial site during smoggy period. Environ. Sci. Eur. 32, 134. https://doi.org/10.1186/s12302-020-00420-9.

Pike, C.R., Roberts, A.P., Verosub, K.L., 1999. Characterizing interactions in fine magnetic particle systems using first order reversal curves. J. Appl. Phys. 85, 6660–6667.

Rachwał, M., Wawer, M., Jabłońska, M., Rogula-Kozłowska, W., Rogula-Kopiec, P., 2020. Geochemical and mineralogical characteristics of airborne particulate matter in relation to human health risk. Minerals 10, 866. https://doi.org/10.3390/min10100866.

Revuelta, M.A., McIntosh, G., Pey, J., Perez, N., Querol, X., Alastuey, A., 2014. Partitioning of magnetic particles in PM10, PM2.5 and PM1 aerosols in the urban atmosphere of Barcelona (Spain). Environ. Pollut. 188, 109–117. https://doi.org/10.1016/j.envpol.2014.01.025.

Roberts, A.P., Tauxe, L., Heslop, D., Zhao, X., Jiang, Z., 2018. A critical appraisal of the "Day" diagram. J. Geophys. Res.: Solid Earth 123, 2618–2644. https://doi.org/10.1002/2017JB015247.

Roberts, A., Pike, C.R., Verosub, K.L., 2000. First-order reversal curve diagrams: a new tool for characterizing the magnetic properties of natural samples. J. Geophys. Res. 105, 28461–28475.

Rovetta, A., 2021. The impact of COVID-19 lockdowns on particulate matter emissions in Lombardy and Italian citizens' consumption habits. Front. Sustain. 2, 649715. https://doi.org/10.3389/frsus.2021.649715.

Sagnotti, L., Macrì, P., Egli, R., Mondino, M., 2006. Magnetic properties of atmospheric particulate matter from automatic air sampler stations in Latium (Italy): toward a definition of magnetic fingerprints for natural and anthropogenic PM10 sources. J. Geophys. Res. 111, B12S22. https://doi.org/10.1029/2006JB004508.

Sagnotti, L., Winkler, A., 2012. On the magnetic characterization and quantification of the superparamagnetic fraction of traffic-related urban airborne PM in Rome, Italy. Atmos. Environ. 59, 131–140.

Sagnotti, L., Taddeucci, J., Winkler, A., Cavallo, A., 2009. Compositional, morphological, and hysteresis characterization of magnetic airborne particulate matter in Rome, Italy. G-cubed 10 (8). https://doi.org/10.1029/2009GC002563 n/a-n/a.

Shu, J., Dearing, J.A., Morse, A.P., Yu, L.Z., Yuan, N., 2001. Determining the sources of atmospheric particles in Shanghai, China, from magnetic and geochemical properties. Atmos. Environ 35, 2615–2625.

Spassov, S., Egli, R., Heller, F., Nourgaliev, D.K., Hannam, J., 2004. Magnetic quantification of urban pollution sources in atmospheric particulate matter. Geophys. J. Int. 159, 555–564.

Szönyi, M., Sagnotti, L., Hirt, A.M., 2007. On leaf magnetic homogeneity in particulate matter biomonitoring studies. Geophys. Res. Lett. 34, L06306. https://doi.org/10.1029/2006GL029076.

Szönyi, M., Sagnotti, L., Hirt, A.M., 2008. A refined biomonitoring study of airborne particulate matter pollution in Rome, with magnetic measurements on Quercus Ilex tree leaves. Geophys. J. Int. 173, 127–141.

Thompson, R., Oldfield, F., 1986. Environmental Magnetism. Allen and Unwin, 978-0-04-538003-9.

Winkler, A., Caricchi, C., Guidotti, M., Owczarek, M., Macrì, P., Nazzari, M., Amoroso, A., Di Giosa, A., Listrani, S., 2019. Combined magnetic, chemical and morphoscopic analyses on lichens from a complex anthropic context in Rome, Italy. Sci. Total Environ. 690, 1355–1368.

Winkler, A., Contardo, T., Vannini, A., Sorbo, S., Basile, A., Loppi, S., 2020. Magnetic emissions from brake wear are the major source of airborne particulate matter bioaccumulated by lichens exposed in milan (Italy). Appl. Sci. 10, 2073. https://doi.org/10.3390/app10062073.